



# FE modeling for ultimate behavior predictions of RC beam

Pandimani<sup>1</sup> · Yeduvaka Damodara Rao<sup>1</sup> · Ijada Gopala Krishna<sup>1</sup>

Received: 10 June 2023 / Accepted: 22 June 2023 / Published online: 2 July 2023  
© The Author(s), under exclusive licence to Springer Nature Switzerland AG 2023

## Abstract

This study encompasses a Finite Element (FE) analysis simulation approach and assessment of ultimate behavior responses of the Reinforced Concrete (RC) beam using the Analysis System (ANSYS) tool. The configuration of the 3D beam model is generated in APDL graphical user interface for validation. The developed FE model used smear-type cracks for concrete and a discrete reinforcement method for steel bars. The crushing and cracking phenomenon of the FE beam is modeled using William and Warnke's method and Von-mises failure criteria. The FE analysis load–deflection plots are corroborated through the available tested curves in the literature, and it found that both curves are in accordance. The FE evaluated ultimate results show a maximum disparity of 9% with the tested beam results. The average ratio of numerically predicted yield load and deflection with the experimental beam are 1.05 and 1.07, respectively. The average percentage of numerically evaluated ultimate load capacity and deflection exhibit 1.07 and 1.01, respectively, against the experimental beam. Furthermore, the numerically validated model is used to examine the flexural response under different strain magnitudes ( $\epsilon_{tn}$ ) of tensile reinforcement at the nominal stage. The transition-controlled (TRC) and compression-controlled (CC) beam predicted an ultimate moment capacity of 61.42 and 92.92% higher than those of tension-controlled (TRC) beams. The TRC and CC beams showed a 35.54 and 62% reduction in ductility against the TC beam.

**Keywords** Flexural capacity of RC beam · Numerical modeling · Limiting strain of tensile reinforcement · Free-vibration response · Crack evolution

## Abbreviations

FEA	Finite element analysis
APDL	ANSYS parametric design language
$f_{ck}$	Characteristic strength (compressive) of concrete
$A_s$	Area of tensile steel bar
$d$	Beam effective depth
IS	Indian standard
$M_n$	Nominal moment
$X_u$	Depth of neutral axis
$E_c$	Elasticity modulus of concrete
$f_t$	Maximum strength (tensile) of concrete
$P_y$	Beam yield load
$\Delta_y$	Beam yield deflection
$P_u$	Beam ultimate load
$\Delta_u$	Beam ultimate deflection
$\beta_t$	Shear transfer coefficient

TC	Tension-controlled section
TRC	Transition-controlled section
CC	Compression-controlled section

## Introduction

Evaluation of ultimate moment resistance and deflection response and nonlinear behavior of structural elements like beams is usually made by experimental study. An experimental investigation becomes laborious, and only limited results can be obtained. On the other hand, methods like numerical analysis deliver comprehensive results at each loading interval up to the failure stage. Numerical analysis can be a perfect alternate substitute for the highly complicated and cost involving experimental methods (Kaveh, 2014; Kaveh et al., 1998; Pandimani et al., 2023). Evaluation of load–deflection response and crack progression at crack initiation, yielding, and ultimate stage, and the complete nonlinear response up to the failure stage, can be efficiently predicted by the FE software. The mathematical modeling for linear and nonlinear material properties and various

✉ Pandimani  
mani.p@gmrit.edu.in

<sup>1</sup> Department of Civil Engineering, GMR  
Institute of Technology, Vizianagaram District,  
Andhra Pradesh 532127 Rajam, India

constitutive models are presented. This study represents the capability of the FE method for assessing the ultimate behavior response of RC beams using the versatile numerical tool. ANSYS is a robust and sophisticated numerical tool that predicts satisfactory results. This study provides ANSYS software's comprehensive material and cracks modeling aspects and nonlinear simulation strategies to examine the bending response under two-point loadings. Perfect bond (no sliding) condition is assumed at the interface between concrete and reinforcement, and concrete's nonlinear tensile stiffening behavior is incorporated into the FE models. Various material constitutive laws are incorporated into the numerical model, representing the experimental beam's different element properties. The responses, like the load–deflection plot and the load and deflection magnitude at the failure of the developed model, are validated with the data of the tested RC beam adapted from the previously published article. Besides the FE modeling approach, three additional RC beam models are generated to investigate the flexure response of tension, transition, and compression-controlled beam section. Later, the predicted numerical moments at failure are verified with the theoretical expression based on two national code provisions. The code expression gives a nearer prediction and closer agreement with the numerical results. Generally, free vibration analysis assesses the preliminary information required for extended dynamic analysis. To investigate the mode shape and natural frequency under free vibration response, under various strain limits as well as a varying area of tensile steel reinforcements, five more numerical models are generated from each category of RC beam. The natural frequency and the displacement results are compared with each other. From the past literature studies, it is identified that several researchers and scholars have used the ANSYS FE analysis tool to corroborate their tested results and extended the numerical analysis for various effective parameters on the RC beam's bending response. A numerical simulation is done through an analysis tool to probe the beam's flexure conduct reinforced with an Aramid fiber bar (Buyukkaragoz et al., 2013). The predicted results, like load and deflections, correlate well with the other two studies. Vasudevan et al., 2013 studied the nonlinear response of medium and high grades of concrete beams using the ANSYS software (Vasudevan et al., 2013). The FE models are capable of predicting the ultimate failure and correlate well against the tested results. A computational study is performed with two loading methods, namely load control and displacement control methods for RC beam (Osman et al., 2017; Yousuf et al., 2017). The authors performed the analysis using both methods separately and verified the computational results with the results of the tested beam presented in past works. The authors concluded that the displacement control method gives stiffer load–deflection results than the force method. A numerical

study is conducted to corroborate the experimental hybrid steel-FRP reinforced concrete beams (Bui et al., 2018). The authors further extended their study by using the validated numerical models and explored the ductility behavior of hybrid reinforcements under many impact aspects. The influence of unsymmetrical bending of beams with carbon FRP rods under shear behavior is executed numerically (Hawileh et al., 2019). The authors stated that the numerical model is consistent for assessing the capacity of carbon FRP beams in shear, and the results are in good relation to the tested beam data. An experimental study and numerical investigation were conducted to assess the deflection response of beams that had pre-existing cracks and renovated RC beams (Hamrat et al., 2020). The FE-evaluated load–deflection plots are verified with the tested (RC) beams for different FRP sheet types and the number of layers. Hybrid concrete beams containing self-compacting high-strength concrete matrix in the compression region and normal-grade concrete in the tension region are tested experimentally (Hussain et al., 2021). The authors studied the influence of the thickness of the concrete layer over the compression region and the shear reinforcements for a maximum capacity of hybrid beams. The tested beam results are later compared with the numerical models and stated that the load–deflection plots are in good agreement. Kaya & Ozcar, 2021 analyzed the one-way slab under the influence of openings using the FE model (Kaya and Anil, 2021). The predicted numerical results are verified against the author's tested beam data and demonstrated that the FE model predicts closer results. Numerous numerical models are generated using the ANSYS tool to compare the existing results of experimental data in the literature (Pandimani et al., 2021a,b, Kaveh et al., 1998; Pandimani, 2023). The validated beam model is utilized later to explore several significant aspects which altered the flexural performance of RC beams. Several authors have used the artificial neural network (ANN) approach to determine the maximum load-resisting capacity of RC beams (Kaveh, 2014). Among those, Rafooei et al., 2011, used the ANN approach to assess the susceptible damage of concrete buildings under seismic forces. Two-dimensional buildings with varying story heights and numbers were designed using Iranian code. The damage assessment of the building is evaluated through dynamic nonlinear analysis (Rafooei et al., 2011). Kaveh et al., 2021, did a comparative study using different machine-learning methods to evaluate the buckling strength of composite cylinders. These techniques are used to develop a relationship between the buckling strength with the fiber orientation (Kaveh et al., 2021). Kaveh & Khavaninzadeh, 2023, studied the strength of an axially loaded concrete column with CFRP fibers. The authors used different algorithms to predict the strength of concrete with carbon fibers (Kaveh & Khavaninzadeh, 2023). Kaveh & Khalegi, 1980, analyzed the strength of admixed and plain concrete

using the ANN method. Using this approach, the authors ascertained the compressive strength at 7 and 28 days for several trials mixes (Kaveh et al., 1998). Though the ANSYS and ANN models are used in past analysis work for assessing the flexural response of RC beams. In this study, the author implemented the ANSYS model over the ANN model for the following reasons: (i) the ANN model can only analyze the beam behavior but can't provide a graphical display of the output result. (ii) The ANN model can't display the crack evolution and progression of RC beams.

### Modeling methodology

This section presents the complete linear and nonlinear mathematical and crack modeling approach of RC beams in the ANSYS domain. The nonlinear material behavior, concrete failure criteria, and iteration procedures are explained comprehensively.

#### Concrete linear behavior modeling

The concrete's elastic linear property is defined by Poisson's ratio and elasticity modulus (Hawileh, 2015; Sayed, 2009; Xiaoming & Hongqiang, 2012). The elastic modulus (E) is defined by using the expression  $4700 \sqrt{f'_c}$ , and 0.2 Poisson ratio ( $\nu$ ) is assigned for concrete (ACI, 2019). The isotropic material stress–strain matrix is given in Eq. (1).

$$[D^c] = \frac{E}{(1 + \nu)(1 - 2\nu)} \begin{bmatrix} (1 - \nu) & \nu & \nu & 0 & 0 & 0 \\ \nu & (1 - \nu) & \nu & 0 & 0 & 0 \\ \nu & \nu & (1 - \nu) & 0 & 0 & 0 \\ 0 & 0 & 0 & \frac{(1-2\nu)}{2} & 0 & 0 \\ 0 & 0 & 0 & 0 & \frac{(1-2\nu)}{2} & 0 \\ 0 & 0 & 0 & 0 & 0 & \frac{(1-2\nu)}{2} \end{bmatrix} \quad (1)$$

#### Concrete nonlinear behavior modeling

Desayi and Krishnan's model, as represented by Eq. (25), is employed to define the concrete stress–strain response in compression (Godinez et al., 2015; Ozcan et al., 2009). This single expression represents the rising and falling curve profile, as illustrated in Fig. 3a. A concrete stress–strain (tri-linear) relationship in tension is represented by the ANSYS default model, as shown in Fig. 3b (Ansys, 2016). The model linearly rises upward till rupture (tensile) strength and then vertically descends to 0.6 times the maximum tensile strength. Finally, it linearly drops to zero stress when the strain magnitude is six times the maximum strain, as depicted in Fig. 3b (Pandimani et al., 2022a, b). The maximum strain (compressive) of 0.003 is assumed in this study. The failure model adopted by ANSYS

well predicts the cracking and crushing failure modes of brittle material like concrete. Equation (2) can represent the concrete failure stress (multi-axial) (Ansys, 2016).

$$\frac{F}{f_c} - S \geq 0 \quad (2)$$

where  $F$  = principal stress function,  $S$  = failure surface.

Five parameters, such as  $f_1$ ,  $f_2$ ,  $f_c$ ,  $f_b$ , and  $f_{cb}$ , are needed to specify the failure surface. However, only  $f_c$  and  $f_t$  constants are sufficient to define the failure surface (Godinez et al., 2015; Pandimani et al., 2021(a,b)). The remaining constants can be defaulted based on William and Warnke's model as given through Eqs. (3) to (5) (William, 1975).

$$f_1 = 1.45f_c \quad (3)$$

$$f_{cb} = 1.2f_c \quad (4)$$

$$f_2 = 1.725f_c \quad (5)$$

The above-specified equations are said to be effective when the  $|\sigma_h| \leq \sqrt{3} f_c$ . Where,  $|\sigma_h|$  = Hydrostatic stress state =  $\frac{1}{3}(\sigma_{xp} + \sigma_{yp} + \sigma_{zp})$ . When crushing strength ( $f_c$ ) is equal to  $-1$  (i.e., turned off) and when principal stress components exceed  $f_t$ , the material initiates cracking. The  $F$  and  $S$  can be defined based on principal directions ( $r_1, r_2$ , and  $r_3$ ) (Pandimani & Geddada, 2022), where:

$$\sigma_1 = \max(\sigma_{xp}, \sigma_{yp}, \sigma_{zp}) \quad (6)$$

$$\sigma_1 = \min(\sigma_{xp}, \sigma_{yp}, \sigma_{zp}) \quad (7)$$

$$\sigma_1 \geq \sigma_2 \geq \sigma_3 \quad (8)$$

where  $f_t$  = maximum (cracking) stress,  $f_c$  = maximum (crushing) stress,  $f_{cb}$  = maximum biaxial stress in compression,  $f_1$  = biaxial (compressive) stress overlaid on the hydrostatic state of stress,  $f_2$  = ultimate (compressive) stress overlaid on the hydrostatic state of stress, and  $r_{xp}, r_{yp}$ , and  $r_{zp}$  = direction of principal stress. The concrete's failure surface can be categorized into 4 categories as illustrated in Eqs. (9) to (12) respectively (Ansys, 2016).

##### 1. Comp-Comp-Comp

$$0 \geq \sigma_1 \geq \sigma_2 \geq \sigma_3 \quad (9)$$

##### 2. Ten-Comp-Comp

$$\sigma_1 \geq 0 \geq \sigma_2 \geq \sigma_3 \quad (10)$$

##### 3. Ten-Ten-Ten

$$\sigma_1 \geq \sigma_2 \geq 0 \geq \sigma_3 \quad (11)$$

##### 4. Ten-Ten-Ten

$$\sigma_1 \geq \sigma_2 \geq \sigma_3 \geq 0 \tag{12}$$

The surface of failure for biaxial stress state in 3-D is represented in Fig. 1. Which reveals that when the nonzero stresses (principal) in  $\sigma_{yp}$  and  $\sigma_{xp}$  directions, three possible surfaces exist that are  $\sigma_{zp}=0$ ,  $\sigma_{zp}>0$ , and  $\sigma_{zp}<0$ . The failure type of material is dependent on  $\sigma_{zp}$ . For example, when  $\sigma_{zp}$  is positive, and  $\sigma_{yp}$  and  $\sigma_{xp}$  both are - ve, cracking may typically occur in the  $\sigma_{zp}$ -direction. But, when  $\sigma_{zp}=0$  or -ve, concrete crushes occur (Al-Rousan, 2020).

### Crack modeling of concrete

Altering the stress–strain relationship by presenting a weak plane perpendicular to the crack face, cracking can be modeled at the integration point. Besides, the reduction in shear strength at the crack face is taken care of by a shear retention coefficient ( $\beta_s$ ). Then the stress–strain matrix concrete in unidirectional is given in Eq. (13).

$$[D_C^{CK}] = \frac{E}{1+v} \begin{bmatrix} \frac{R_t'(1-v)}{E} & 0 & 0 & 0 & 0 & 0 \\ 0 & \frac{1}{1-v} & \frac{v}{1-v} & 0 & 0 & 0 \\ 0 & \frac{v}{1-v} & \frac{1}{1-v} & 0 & 0 & 0 \\ 0 & 0 & 0 & \frac{\beta_s}{2} & 0 & 0 \\ 0 & 0 & 0 & 0 & \frac{1}{2} & 0 \\ 0 & 0 & 0 & 0 & 0 & \frac{\beta_s}{2} \end{bmatrix} \tag{13}$$

When the KEYOPT (7) of the SOLID65 element = zero,  $R_t$  becomes zero, and when it is equal to 1,  $R_t$  becomes a slope, as displayed in Fig. 2.  $R_t$  turns to zero when the solution converges. Where  $T_c$  = stress (tensile) relaxation

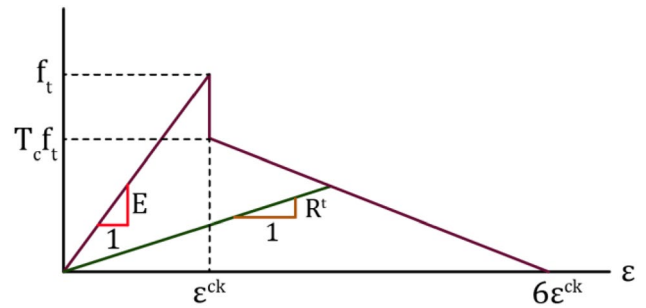


Fig. 2 Strength of concrete under cracked conditions (Ansys, 2016)

factor, which defaults to 0.6. When the crack closes, a coefficient ( $\beta_c$ ) for shear retention is introduced. In this instance, all the stresses (compressive) perpendicular to the crack's plane are transferred through the crack. Consequently, the resulting matrix altered, as given in Eq. (14)

$$[D_C^{CK}] = \frac{E}{(1+v)(1-2v)} \begin{bmatrix} (1-v) & v & v & 0 & 0 & 0 \\ v & 1-v & v & 0 & 0 & 0 \\ v & v & 1-v & 0 & 0 & 0 \\ 0 & 0 & 0 & \frac{\beta_c(1-2v)}{2} & 0 & 0 \\ 0 & 0 & 0 & 0 & \frac{1-2v}{2} & 0 \\ 0 & 0 & 0 & 0 & 0 & \frac{\beta_c(1-2v)}{2} \end{bmatrix} \tag{14}$$

The stress–strain matrix becomes as given in Eq. (15) when the cracking originates along two/three directions, and they are closed.

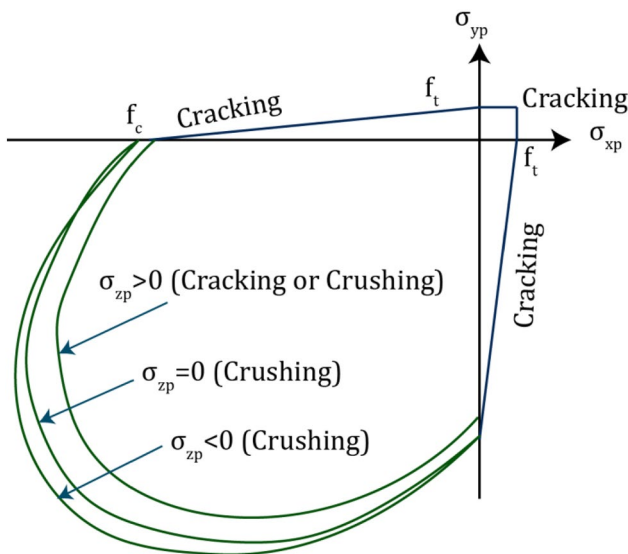


Fig. 1 Failure surface of the concrete in a biaxial stress state (Godinez et al., 2015)

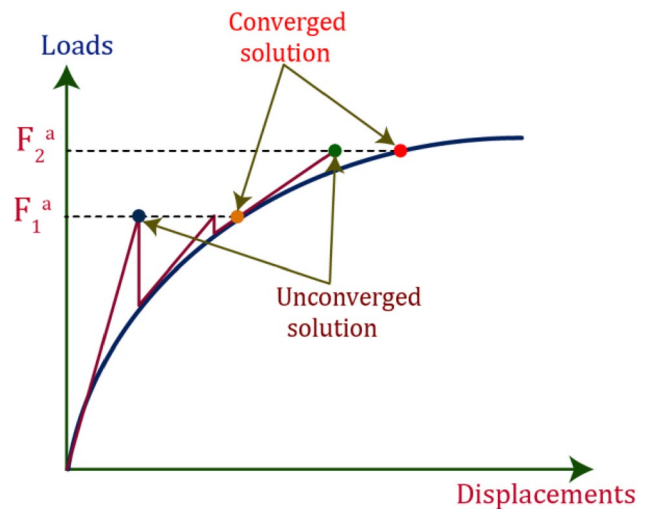


Fig. 3 Newton–Raphson iteration method (Wolanski, 2004)

$$[D_c^{CK}] = E \begin{bmatrix} \frac{R^t}{E} & 0 & 0 & 0 & 0 & 0 \\ 0 & \frac{R^t}{E} & 0 & 0 & 0 & 0 \\ 0 & 0 & 1 & 0 & 0 & 0 \\ 0 & 0 & 0 & \frac{\beta_t}{2(1+\nu)} & 0 & 0 \\ 0 & 0 & 0 & 0 & \frac{\beta_t}{2(1+\nu)} & 0 \\ 0 & 0 & 0 & 0 & 0 & \frac{\beta_t}{2(1+\nu)} \end{bmatrix} \quad (15)$$

The following expression defines the transformation of  $[D_c^{ck}]$  to element coordinates:

$$[D_c] = [T^{ck}]^T [T^{ck}] [D_c^{ck}] \quad (16)$$

where,  $[T^{ck}]$  = transformation matrix. But, the status of cracking (open or closed) depends on a strain  $\epsilon_{ck}^{ck}$ . When no cracking has occurred then,

$$\epsilon_{ck}^{ck} = \epsilon_x^{ck} + \frac{\nu}{1-\nu} \epsilon_y^{ck} + \epsilon_z^{ck} \quad (17)$$

When cracking occurred in the y-direction then,

$$\epsilon_{ck}^{ck} = \epsilon_x^{ck} + \nu \epsilon_z^{ck} \quad (18)$$

When both y and z directions have cracked then,

$$\epsilon_{ck}^{ck} = \epsilon_x^{ck} \quad (19)$$

where,

$\epsilon_x^{ck}$ ,  $\epsilon_y^{ck}$ ,  $\epsilon_z^{ck}$  = normal components of strain in crack direction.

The vector  $\epsilon_x^{ck}$  can be assessed as given in Eq. (20).

$$\{\epsilon_x^{ck}\} = [T^{ck}] \{\epsilon'\} \quad (20)$$

$$\{\epsilon'_n\} = \{\epsilon_{n-1}^{el}\} + \{\Delta \epsilon_n\} - \{\Delta \epsilon_n^{th}\} - \{\Delta \epsilon_n^{pl}\} \quad (21)$$

where, n = number of sub-steps,  $\{\epsilon_{n-1}^{el}\}$  = elastic strain,  $\{\Delta \epsilon_n\}$  = incremental total strain,  $\{\Delta \epsilon_n^{th}\}$  = incremental thermal strain,  $\{\Delta \epsilon_n^{pl}\}$  = incremental plastic strain. When  $\epsilon_{ck}^{ck} < \text{zero}$ , the closing of the crack is assumed, and when  $\epsilon_{ck}^{ck} > \text{zero}$ , the opening of the crack is assumed.

### Non-linear Solutions and convergence criteria

The total load step (applied force) is broken into a sequence of force increments, and each load increment is subdivided into several sub-steps for doing nonlinear iterations. The program default iteration method (Newton–Raphson) is adopted to run the nonlinear analysis (Osman et al., 2017). After each increment of the load step, this iteration method updates the changes that occur in the nonlinearity and is reflected in the stiffness matrix before the subsequent load

step (Wolanski, 2004). The Newton–Raphson method checks the convergence of the solution of each set of load increments within the specified/default tolerance (force/displacement) limits. The iteration process for unidirectional DOF is shown in Fig. 3. An equilibrium equation for nonlinear iteration becomes,

$$\{F^a\} = \{u\}[K] \quad (22)$$

where,  $\{F^a\}$  = applied force,  $\{u\}$  = unknown displacement, and  $[K]$  = stiffness matrix. The nonlinear equation (iterative process) can be modified as given in Eqs. (23) and (24).

$$\{F^a\} - \{F_i^{nr}\} = [K_i^T] \{\Delta u_i\} \quad (23)$$

$$\{u_i\} + \{\Delta u_i\} = \{u_{i+1}\} \quad (24)$$

where,  $\{F_i^{nr}\}$  = restoring force,  $[K_i^T]$  = Jacobian (tangent) matrix, and i = subscript for the current iteration. In this analysis, the automatic (time-stepping) option in the solution control page was adopted for controlling the load increments (Hawileh, 2015). For this (automatic time stepping) option, the user must mention the minimum and maximum number of load increments. The solution convergence looks for minimum load steps if the behavior is smooth and goes for maximum load-step if found to be highly nonlinear. When the solution does not converge, the load increments can be improved, or the sub-step can be altered (Pandimani et al., 2022a,b). The solution generally tends to diverge at the occurrence of the first crack (tensile) or later the reinforcement yielded, which in turn terminates the iterations. A 0.5% and 5% program default tolerance limits for displacement and force vector are assumed initially. But these values are increased later when the solution is difficult to converge due to the high nonlinearity of concrete elements followed by a large displacement. Therefore, the tolerance limits were increased to 10% for force criteria by keeping the displacement limits as program default (Hawileh, 2015; Pandimani et al., 2021a,b). The iteration solution terminates abruptly when the numerical displacements exceed the program default values.

### Finite element modeling of RC beam

Three elements are used to represent the RC beam model in the ANSYS domain. The concrete's crushing and cracking property is simulated using the SOLID65 element, which has 8-node and three translational DOF per node (Ahmad & Saleh, 2022; Choobbor et al., 2019; Mustafa & Hassan, 2018). The elastic–plastic properties of steel reinforcements are represented by two nodes of the LINK180 element, which has 3 DOF per node (Godinez et al., 2015).

To minimize the stress concentration at the support and loading points, an 8-node SOLID185 element is used with 3 DOF per node. To define the stress–strain (compressive) relation of concrete, Desayi and Krishnan's proposed multi-linear curve is adopted, as shown in Fig. 4a (Godinez et al., 2015). The tri-linear stress–strain behavior is assumed to define the tension behavior of concrete by employing the default ANSYS data incorporated with a tensile stress reduction coefficient of 0.6. Steel reinforcements are modeled as bilinear isotropic hardening properties, as shown in Fig. 4b. The constitutive mathematical expressions employed for concrete and steel reinforcements are given in Eqs. (25) to (28) and Eqs. (29) to (30), respectively. The four critical parameters, namely, coefficients for close and open shear strength at the crack, uniaxial cracking, and uniaxial crushing, concern William and Warnke failure criteria and are incorporated into the FE model (Sayed, 2019). A value of open and closed shear coefficients  $\beta_t = 1$  and  $\beta_c = 0.3$  is used in this study. The uniaxial cracking is assigned to SOLID65 element based on Eq. (28). In contrast, the uniaxial crushing strength is suppressed ( $f'_c = -1$ ) or turned off to prevent the premature cracking of concrete elements at the loading and support regions (Xiaoming & Hongqiang, 2012). Two boundary (displacement) conditions are required to restrain the model, similar to the experimental beam. A pinned and roller supports are achieved for the FE model by employing zero displacement constraints in x, y, z, and y-directions, respectively, as displayed in Fig. 7. The loads are applied monotonically above the loading plates until the beam failure occurs by crushing. No real constant is needed for the concrete element since the reinforcements are embedded inside the concrete element using the discrete reinforcement method (Mustafa & Hassan, 2018). The elastic, perfect behavior with the isotropic hardening property of steel

reinforcement is shown in Fig. 5. The real constant in the form of the cross-section area is assigned for steel reinforcements, as presented in Table 1. The linear and nonlinear material properties required for the steel bars and concrete elements of the RC beam are shown in Table 2.

$$f = \frac{E_c \epsilon}{1 + \left(\frac{\epsilon}{\epsilon_0}\right)^2} \tag{25}$$

$$\epsilon_0 = \frac{2f'_c}{E_c} \tag{26}$$

$$E_c = \frac{f}{\epsilon} \tag{27}$$

$$f_t = 0.62\sqrt{f'_c} \tag{28}$$

Where:  $f$  = stress concern to strain ( $\epsilon$ ),  $\epsilon_0$  = maximum compressive strain,  $\epsilon$  = strain concern to stress ( $f$ )

$$f_s = \epsilon_s E_S, \text{ when } \epsilon_s < \epsilon_y \tag{29}$$

$$f_s = f_y = \epsilon_y E_S, \text{ when } \epsilon_s \geq \epsilon_y \tag{30}$$

where  $f_s$  = steel reinforcements stress (MPa) at  $\epsilon_s$ ,  $f_y$  = steel bar yield stress (MPa),  $\epsilon_s$  = strain concern to stress,  $f_s$ ,  $\epsilon_y$  = strain at yielding and  $E_S$  = steel elastic modulus (MPa).

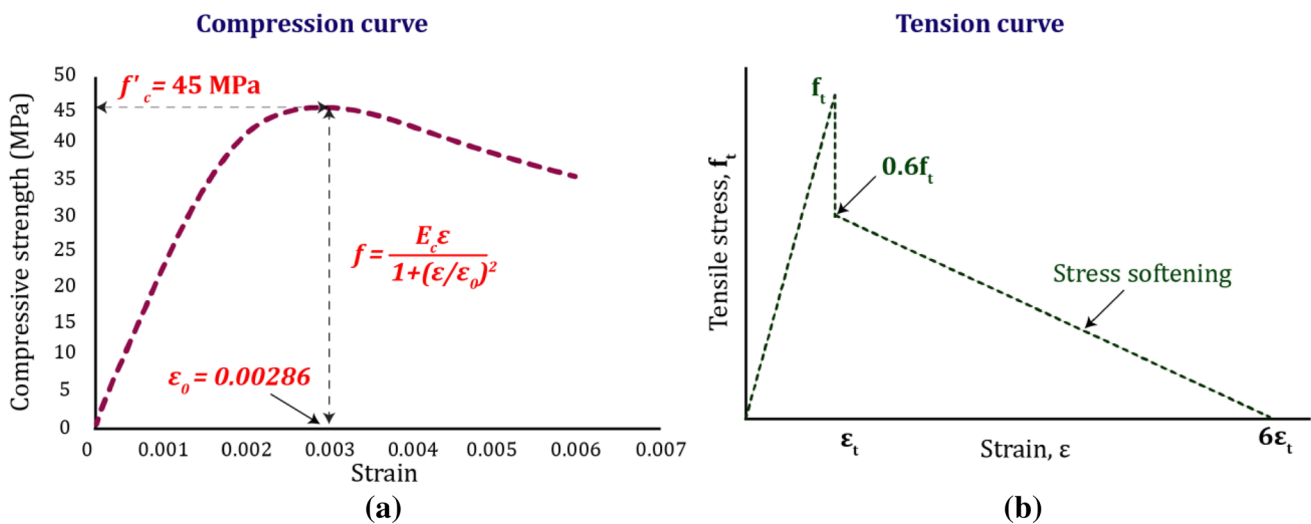


Fig. 4 Constitutive stress–strain model for concrete (Vasudevan et al., 2013)

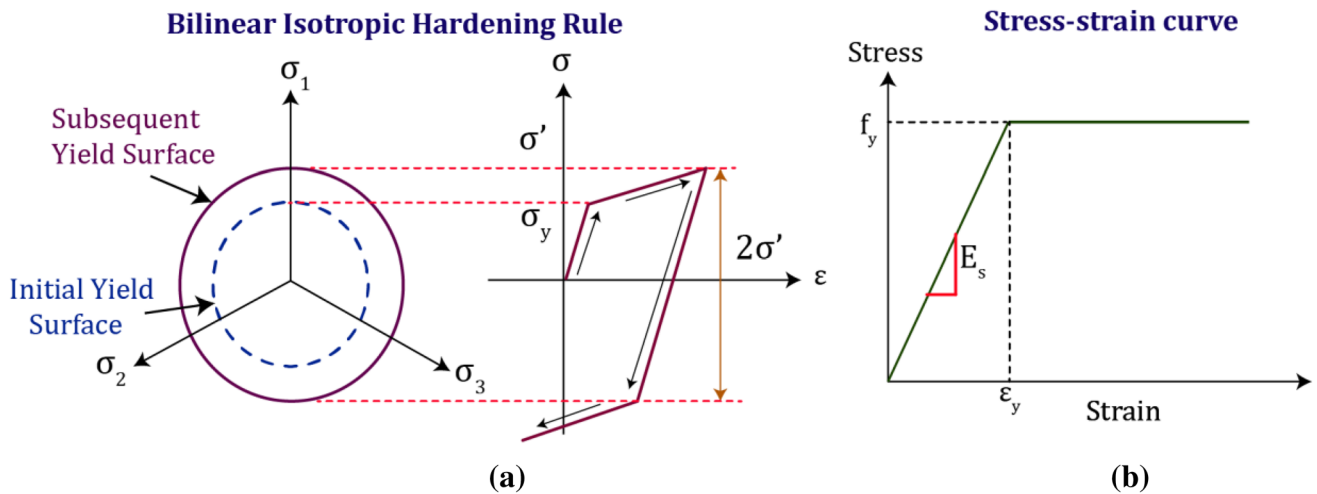


Fig. 5 Reinforcement constitutive model (Godinez et al., 2015)

Table 1 Real constants used for different elements

Real constant set	Element type	Real constants			
1	Solid65		Rebar1	Rebar2	Rebar3
		Material number	0	0	0
		Volume ratio	0	0	0
		Orientation angle	0	0	0
2	Link180 (Main steel)	Beam type	B-10	B-12	B-16
		Cross-section area (mm <sup>2</sup> )	78.53	113.097	201.06
		Initial strain	0	0	0
3	Link180 (Hanger bar)	Cross-section area (mm <sup>2</sup> )	78.53	78.53	78.53
		Initial strain	0	0	0
4	Link180 (Stirrups)	Cross-section area (mm <sup>2</sup> )	50.27	50.27	50.27
		Initial strain	0	0	0

### Verification of numerical (RC) beam

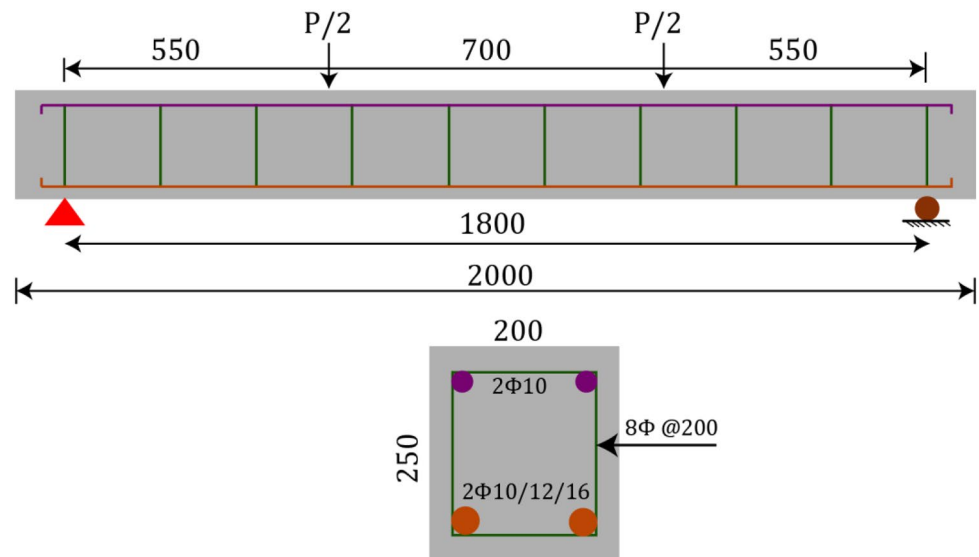
Validations of the developed numerical model are done by comparing the FE analysis results with the experimentally tested beams (Vasudevan & Kothandaraman, 2014). The authors studied the conduct of RC beams externally retrofitted by bars at the bottom. Twenty beams are tested with different internal and retrofitted reinforcement steel bar ratios for normal and high-strength concrete beams. Among those three high-grade and three normal grades, RC beams are kept as conventional beams. In this study, three beams of 35 MPa compressive strength having 250 mm depth, 200 mm width, and 2000 mm span are selected from Vasudevan et al. experimental study (Vasudevan & Kothandaraman, 2014). The three RC beams are reinforced with two main bars with varying diameters of 10, 12, and 16 mm, respectively. The beams have shear

reinforcement of 8 mm diameter at 200 mm c/c spacing and 2-10 mm diameter compression bars. The yield strength of 556 MPa was used for all reinforcements. The configuration of experimentally tested and numerical developed models for RC beams is presented in Figs. 6 and 7, respectively Tables 3 and 4.

The load-resisting capacity at the yielding and ultimate stage predicted by the established models are validated against the experimentally tested data as revealed in Tables 5 and 6. The ratio of the predicted maximum capacity to the experimental maximum capacity shows 1.02, 1.07, and 1.08 for B-10, B-12, and B-16 RC beams. The FE evaluated maximum deflections of the FE model B-10, FE model B-12, and FE model B-16 show 1.04, 1.09, and 1.08 times the ultimate deflections of experimental beams. It is obvious from Table 1 that the numerical ultimate results show a maximum difference of 9%

**Table 2** Element material properties used in ANSYS

Material model number	Element type	Material properties	
1	SOLID65	Concrete element	
		Linear properties	
		EX	EX
		PRXY	0.2
		Nonlinear properties	
		Idealized stress–strain curve	Figure 4a
		Open shear transfer coefficient	0.3
		Closed shear transfer coefficient	1
		Uniaxial cracking stress	3.71 N/mm <sup>2</sup>
		Uniaxial crushing stress	– 1 (turn off)
2	LINK180	Steel reinforcement element	
		Linear properties	
		EX	200,000 N/mm <sup>2</sup>
		PRXY	0.3
		Nonlinear properties	
		Yield stress	525 N/mm <sup>2</sup>
3	SOLID185	Tang modulus	20 N/mm <sup>2</sup>
		Loading and support plate element	
		Linear properties	
		EX	200,000 N/mm <sup>2</sup>
		PRXY	0.3

**Fig. 6** Details of the experimental beam (Vasudevan & Kothandaraman, 2014)

related to the experimentally tested beams. The ratios of yield load and the ratio of deflection predicted by the FE model B-10, FE model B-12 and FE model B-16 show 1.07 and 0.97, 1.10 and 1.13, and 1.05 and 0.94 respectively with the experimental result. The validations

of the ultimate load–deflection response profile of the numerical model and the tested beam are presented in Fig. 8, which reveals that both curves are in good agreement. The predicted ultimate load capacity is increased whereas the ductility index decreases when the steel area



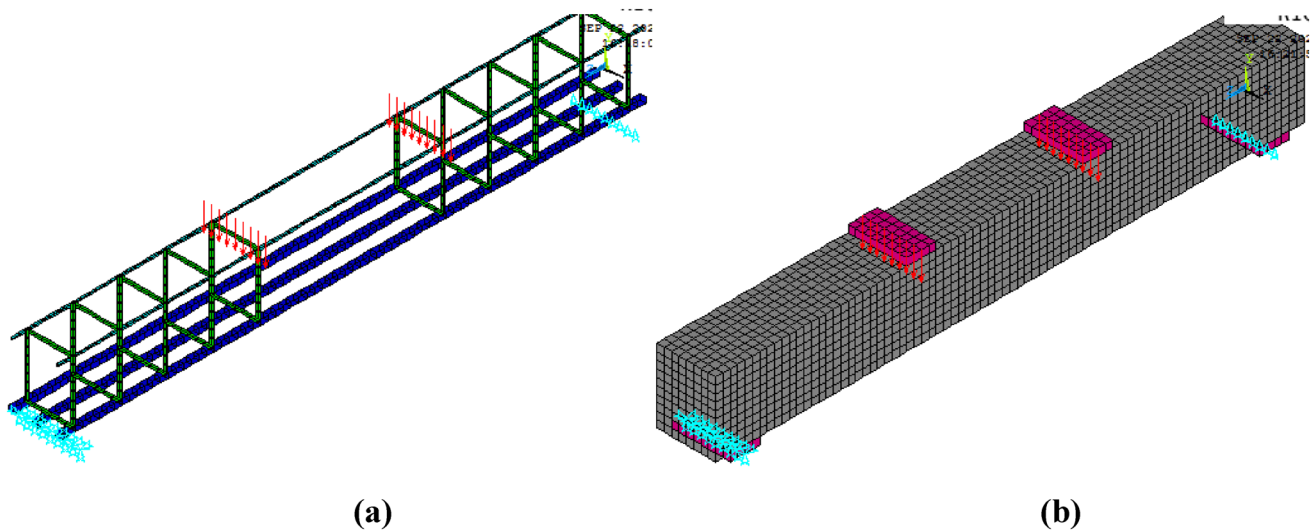


Fig. 7 Proposed numerical model: **a** Reinforcement model and **b** Concrete model

**Table 3** Comparison of experimental and numerical results at yield load

Beams	Yield load, $P_y$ (kN)		Ratio	Yield deflection, $\Delta_y$ (mm)		ratio
	Exp	FEA		Exp	FEA	
B-10	65.09	69.75	1.07	6.02	5.84	0.97
B-12	74.90	82.62	1.10	5.56	6.26	1.13
B-16	145.09	151.90	1.05	8.10	7.63	0.94

**Table 4** validation of experimental and numerical ultimate results

Beams	Ultimate load, $P_u$ (kN)		ratio	Ultimate deflection, $\Delta_u$ (mm)		ratio
	Exp	FEA		Exp	FEA	
B-10	75.41	76.70	1.02	18.51	19.23	1.04
B-12	96.12	102.42	1.07	19.22	20.89	1.09
B-16	160.10	173.46	1.08	17.55	18.91	1.08

**Table 5** Moment-deflection comparison at critical points

Beams	$M_{cr}$ (kNm)	$\Delta_{cr}$ (mm)	$M_y$ (kNm)	$\Delta_y$ (mm)	$M_u$ (kNm)	$\Delta_u$ (mm)
TC	21.58	0.65	125.75	6.27	139.90	43.57
TRC	25.27	0.57	211.92	8.25	225.83	36.97
CC	29.35	0.52	233.41	7.91	269.89	20.90

**Table 6** validations of numerical and theoretical ultimate moment capacity

Beams	Ultimate moment-resisting capacity (kN-m)				
	FEA	ACI 318–19	Ratio	IS: 456–2000	Ratio
TC	139.90	126.90	1.10	126.43	1.11
TRC	225.83	211.77	1.06	214.31	1.05
CC	269.89	253.10	0.91	229.02	1.18

is increased; this justifies the similar observation made by Vasudevan et al. experimental study beam (Vasudevan & Kothandaraman, 2014). From the validation study, it is suggested to extend the proposed FE model for further parametric study.

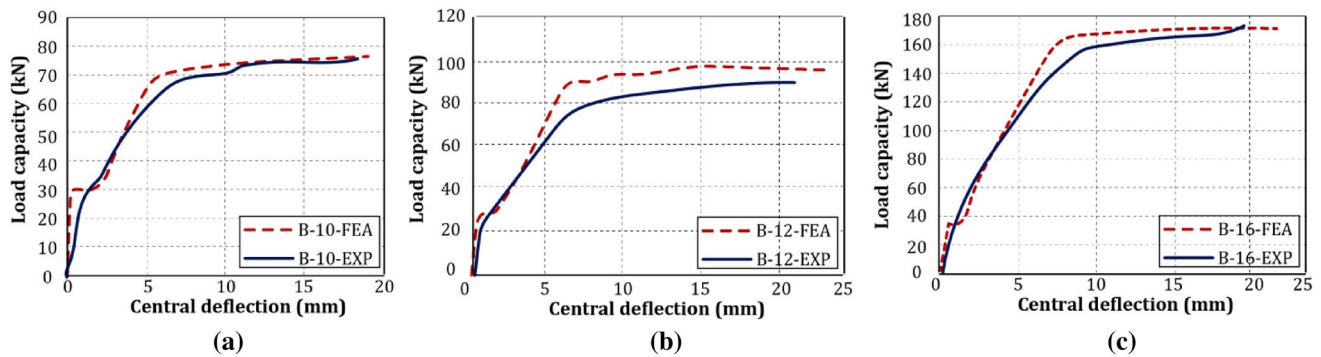


**Fig. 8** Load–deflection response comparison: **a** for the B-10 model, **b** for the B-12 model, and **c** for the B-16 model

## Results and discussions

The verified numerical models are used for further extended study. This section discusses the responses of tension, compression, and transition-controlled RC beams, and the numerically obtained load–deflection curves and magnitudes are compared. Besides, crack generation and progression of RC beams are also presented for these three types of sections.

### Comparison of numerical RC beams

The corroborated numerical models assess the nonlinear response of TC, CC, and TRC beams under four-point loading conditions. As per code ACI 318–19, the RC beams are categorized according to the limiting strain of extreme tensile reinforcement at nominal strength. When the strain is less than or equal to 0.002, greater than 0.005, and between 0.002–0.005, the beam type is considered compression, tension, and transition-controlled section, respectively (ACI, 2019). In this study, the limiting strain of 0.010, 0.0348, and 0.0018 are evaluated theoretically, which in turn gives the tensile reinforcement area of 855.06mm<sup>2</sup>, 1520.12 mm, and 1934.01mm<sup>2</sup> for tension, transition, and compression controlled beams respectively. Based on the area of tensile reinforcement, three FE models are generated to evaluate the load–deflection magnitudes at crucial locations, mid-span load–deflection response curves up to failure, and crack evolution of the concrete beam section. The moments and deflections of the three developed models at the formation of tensile crack, at the yield point, and the final stage of concrete crushing captured through the FE analysis are demonstrated in Table 5. The maximum resisting moment predicted by the FE models was verified with the code expressions, as shown in Table 6. The validation of moment–deflection curves for TC, TRC, and CC beams are depicted in Figs. 9, 10a, b, and c, respectively. The cracking moment has increased by 17.09 and 36% for TRC and CC sections compared to the TC section. A 68.52 and 85.61% yield moment

increment is observed for the TRC and CC sections against the TC sections. The maximum moment resisting capacity of the TRC and CC beam increased by 82.86 and 92.92% compared to the TC beam. The maximum mid-span (verticle) deflection of the TRC and CC beam sections is decreased by 15.15 and 52.02% compared with the TC section. The ductility (displacement) of 6.95, 4.48, and 2.64 is obtained for the TC section, TRC section, and CC section, which reveals that the ductility of RC beams reduced considerably with the increasing area of tensile steel. The proportion of the FE model predicted maximum moment to the ACI code expression shows 1.10, 1.06, and 0.91 for TC, TRC, and CC beams.

Similarly, the numerical predicted ultimate moment ratio to IS: 456 expressions gives 1.11, 1.05, and 1.18 for TC, TRC, and CC beams. It is concluded from Table 6 that both the code expressions exhibit similar results when compared to the FE results. The ultimate deflection captured by the FE model for TC, TRC, and CC beam is presented in Fig. respectively. The supplementary file Fig. S1 (a) to (c) shows the predicted principal stress (tensile) contour diagram at the first (rupture) crack, and Fig. S1 (d) to (f) shows the Von-misses stress contour diagrams at ultimate failures of TC, TRC, and CC beam sections respectively.

### Analytical study

The numerically predicted ultimate moment resisting capacity of tension, transition, and compression-controlled RC beam is verified with the code expression based on the ACI 318–19 and IS 456–2000 (ACI, 2019; IS 456, 2000). The stress–strain relationship and the ultimate load resistance for the RC beam under these two code provisions are represented in Fig. 11. The ultimate moment of resistance expression for the TC, TRC, and CC beam section as per the code ACI 318–19 and for the under, balance and over-reinforced concrete section related to the code IS 456–2000 is presented in Eqs. (31) and (33), respectively (ACI, 2019; IS 456, 2000). The Indian code IS 456–2000 categorized the RC beam as under, balanced,

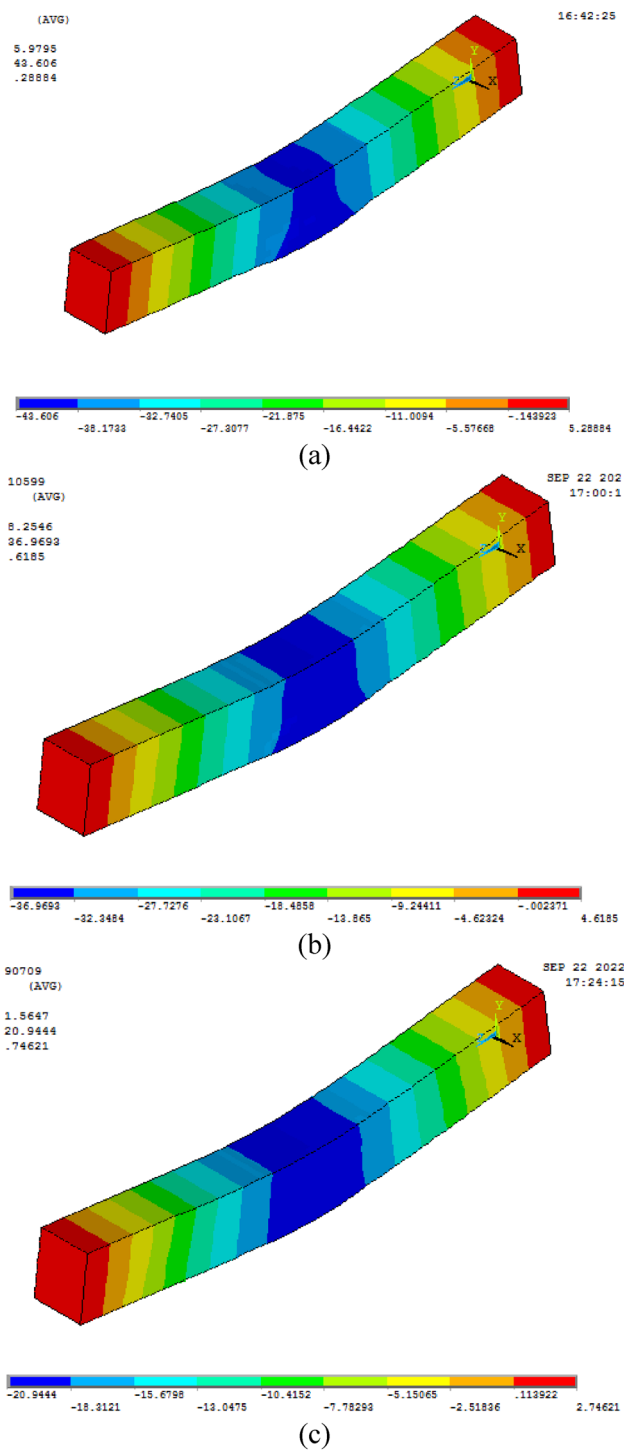


**Fig. 9** Ultimate deflection: **a** TC beam, **b** TRC beam, and **c** CC beam

and over-reinforced sections, following the neutral axis depth (IS 456, 2000). When the limiting depth of the neutral axis is lower than, equal to, or more than the actual neutral axis depth, the beam section is said to be an under, balanced, and over-reinforced beam, respectively. From the ACI 318–19 code:

$$\text{The nominal resistance } (M_n) = f_y A_s (d - 0.5a) \tag{31}$$

$$\text{The stress block depth } (a) = f_y A_s / 0.85 f'_c b \tag{32}$$

From IS 456–2000 code

$$\text{Ultimate moment } (M_u) = f_y A_{st} (d - 0.42 x_u) \tag{33}$$

$$\text{Actual height of neutral axis } (x_u) = A_{st} f_y / 0.542 b f_{ck} \tag{34}$$

### Crack evolution

The first cracking in the concrete element is formed between the loading points at the extreme bottom fiber of the beams. The cracking of concrete elements occurs at the integration points in three perpendicular directions with a circular sign as displayed in Fig. 12. The crack pattern at the ultimate collapse of the RC beam is shown in Fig. 13, where Fig. 13a, b, and c represent the flexural, compression, and diagonal shear types of cracks respectively. Whenever the principal tensile stress of concrete element (SOLID65) exceeds the uniaxial cracking stress of concrete ( $f_t$ ), cracking initiates represented by a circular red-colored sign perpendicular to the longitudinal direction as shown in Fig. 14a, 15a, and 16a. The red, green, and blue colors represent the primary, secondary, and tertiary cracks, as shown in Fig. 13. At first cracking, 21.58kN-m, 25.27kN-m, and 29.35kN-m moments were observed for TC, TRC, and CC beam sections as illustrated in Table 5.

When the numerical model is further loaded, numerous flexural tensile cracks are observed around the pure bending and shear zones. It is witnessed that, at the yield point of the FE model, more diagonal cracks are formed within the shear zone, and then few flexural and shear cracks are propagated towards the compression fiber as shown in Fig. 14b, 15b, and 16b. At the yielding of steel bars, the FE model exhibit 125.75kN-m, 211.92kN-m, and 233.41kN-m, respectively, for TC, TRC, and CC beams, as illustrated in Table 5. Finally, horizontal cracks develop near the top compression fibers when the principal (compressive) stress of SOLID65 elements reaches the concrete maximum compressive stress. At this stage, the beam is assumed to fail by concrete crushing, as shown in Figs. 14c, 15c, and 16c. An ultimate moment capacity of 139.90kN-m, 225.83kN-m, and 269.89kN-m were obtained for TC, TRC, and CC beams, respectively, as shown in Table 5.

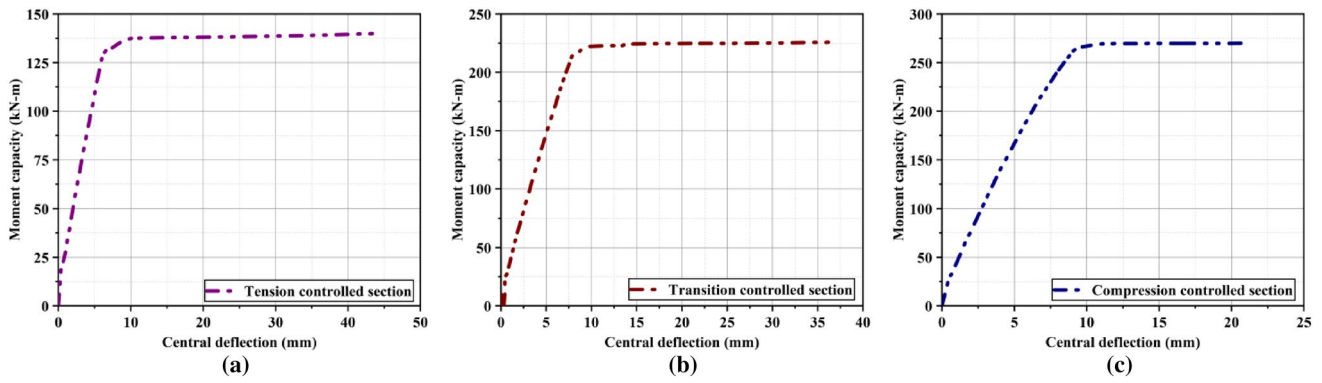


Fig. 10 Moment-deflection curve comparison: a tension-controlled, b transition-controlled, and c compression-controlled models

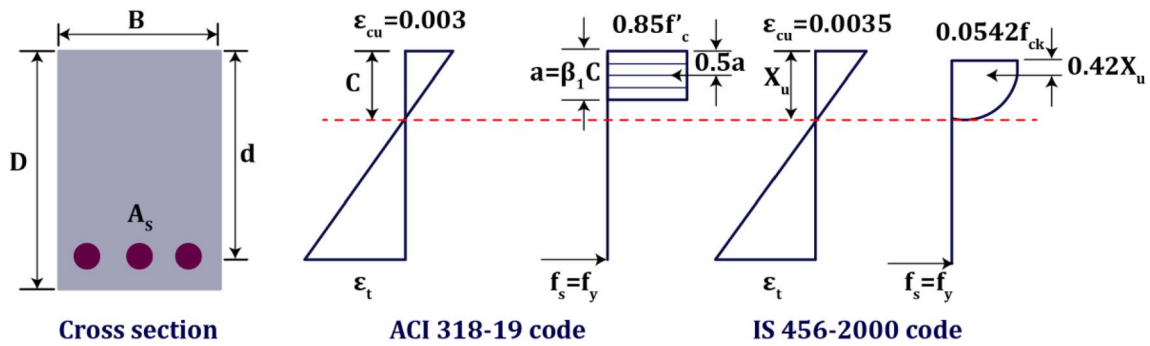


Fig. 11 Stress–strain distribution for RC beams (Pandimani et al., 2021 a, b)

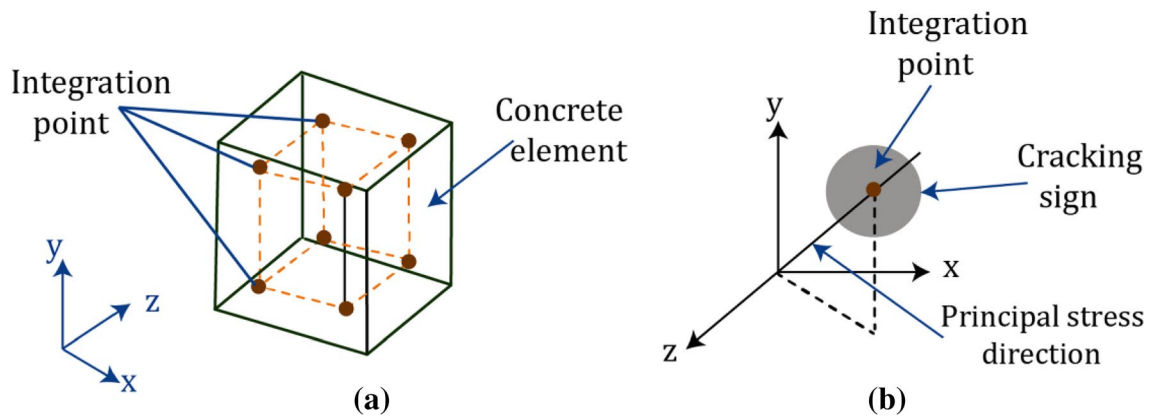


Fig. 12 Crack formation in concrete element: a Integration points and b cracking sign (Ansys, 2016)

**Free vibration analysis**

This section develops nine models with varying strain limits in tensile reinforcements. Three types of sections are formed: tension, transition, and compression-controlled beams. Three models, each from tension, transition, and

compression-controlled beams, are generated with supported ends subjected to free vibration. Only the self-weight of the beams is considered by assigning the weight density and acceleration due to gravity. The free vibration analysis is done under the Block Lanczos method (Ansys, 2016), and the first five natural frequencies and the displacements are determined as shown in Fig. 17. It is observed from Table 7 that all the types of beams have shown nearly similar natural

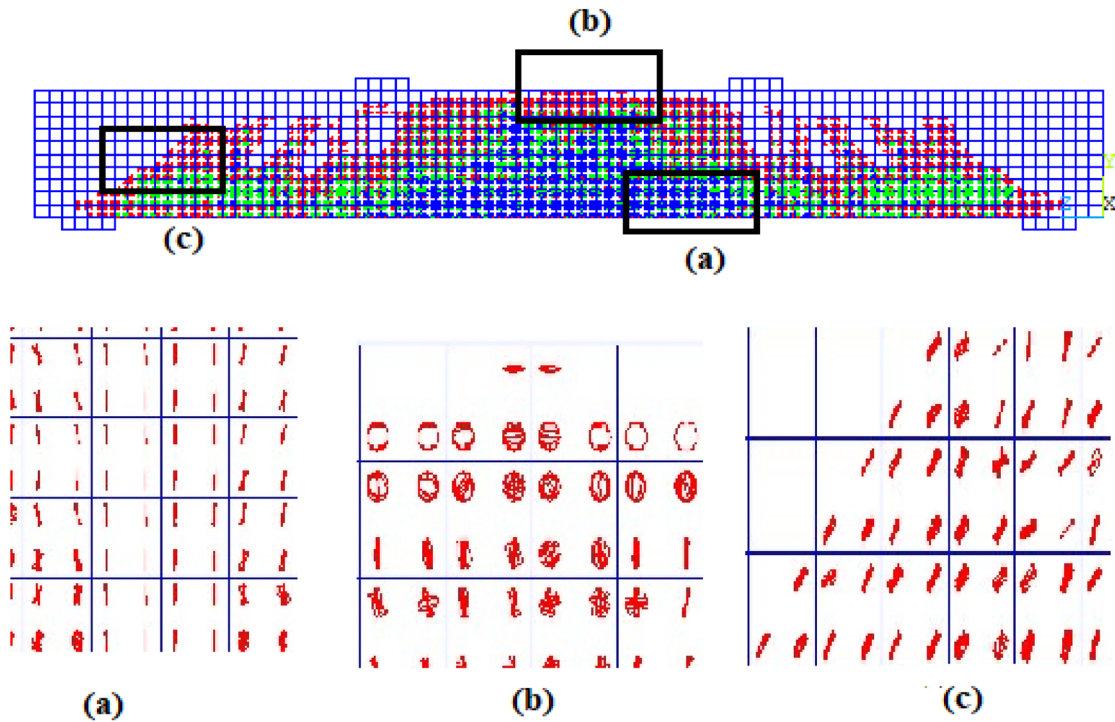
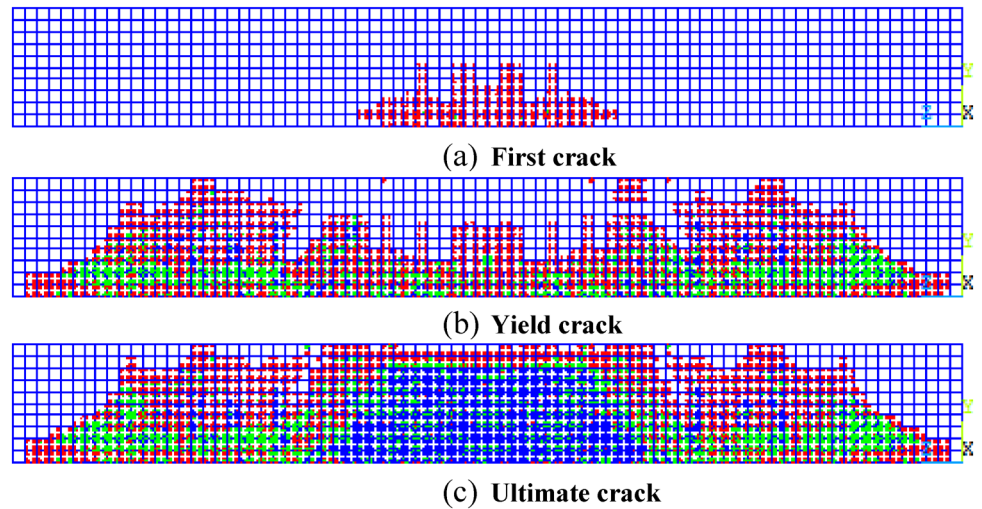


Fig. 13 Various crack formations in the ANSYS beam model

Fig. 14 Concrete crack patterns for TC beam



frequencies and displacement results. This suggests that the strain limit and the area of tensile reinforcement have an insignificant effect on the vibration characteristics. However, the natural frequency increases with the number of mode shapes, and mode 5 predicts the highest frequency. The predicted natural frequency and mode shapes are depicted in Fig. 17.

### Conclusions

This study presents the mathematical modeling approach for the linear or nonlinear response of RC beams. From the numerical analysis, it is evident that the proposed numerical models can capture the nonlinear conduct of the RC beam until its failure with reasonable accuracy. The proposed FE models have a few limitations (1) It does not capture the post-peak response since the input stress–strain curve is assumed to be a horizontal straight line soon after

**Fig. 15** Concrete crack patterns for TRC beam

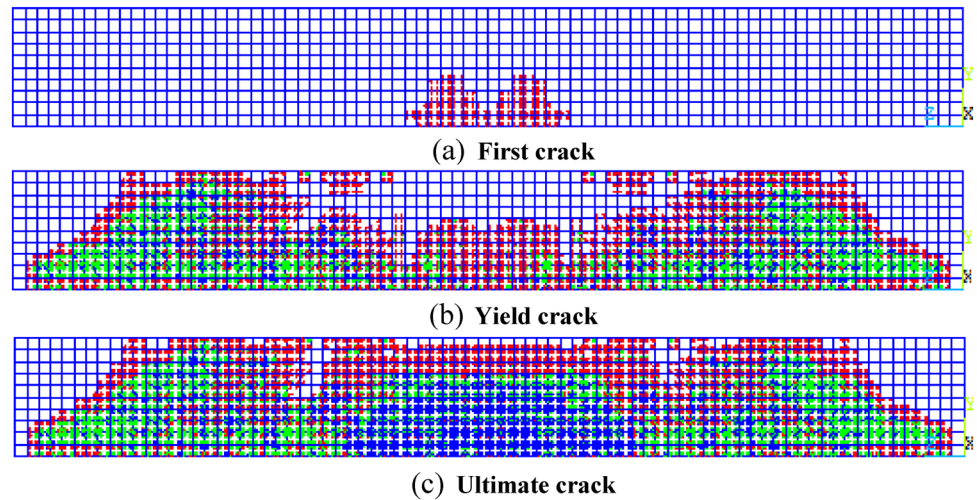
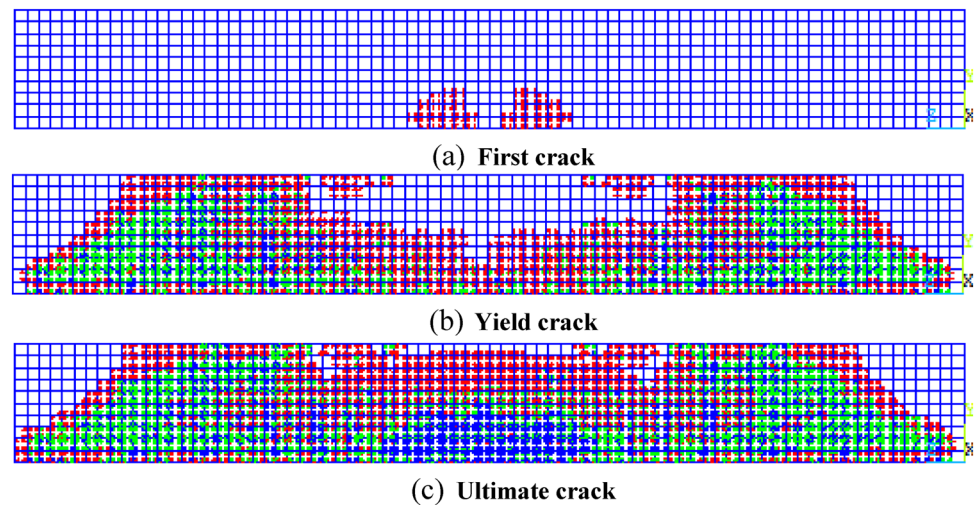


**Fig. 16** Concrete crack patterns for CC beam



the maximum compressive strength. (2) The FE model assumes perfect bond condition, so it cannot assess relative slip of reinforcement. Moreover, the future scope of this study is: (1) The validated model shown in this paper can extensively be used to evaluate the effect of shear and flexure-deficient RC beams under static loadings. (2) It can also be used to study the effect of other special concrete RC beams (like geopolymer concrete beams and high-performance concrete beams). (3) ANN models can be used for validation and comparing their results with the ANSYS models. From this numerical study, the following observations are obtained.

- A) The generated FE model proficiently captures the load–deflection plot, load and deflection results at cracking, yielding, and ultimate stages, and the crack evolution and propagation in concrete.
- B) The crack, yielding, and ultimate moment capacity of TRC and CC beams are found to be 17.10 and 36, 68.52 and 85.61, 61.42, and 92.92% higher magnitude compared to the TC section.
- C) The yield deflection is enhanced by 31.58 and 26.16%, whereas the maximum deflection is declined by 15.14% and 52.03% for the TC beam when compared with the TRC and CC beams, respectively.
- D) The modal analysis determined that the three types of RC beam sections with varying strain limits and tensile steel areas have found insignificant effects on the natural frequency and displacement under free vibration response.
- E) The FE predicted ultimate moment for TC, TRC, and CC beams show 1.10, 1.06, and 0.91 times the theoretically evaluated ultimate moment for ACI code expressions. In contrast, these values become 1.11, 1.05, and 1.18 times the theoretical moments based on IS code expressions.
- F) The ratio of numerical to the experimental moment and deflection results show a maximum deviation of 1.10 and 1.13, respectively, whereas these results become

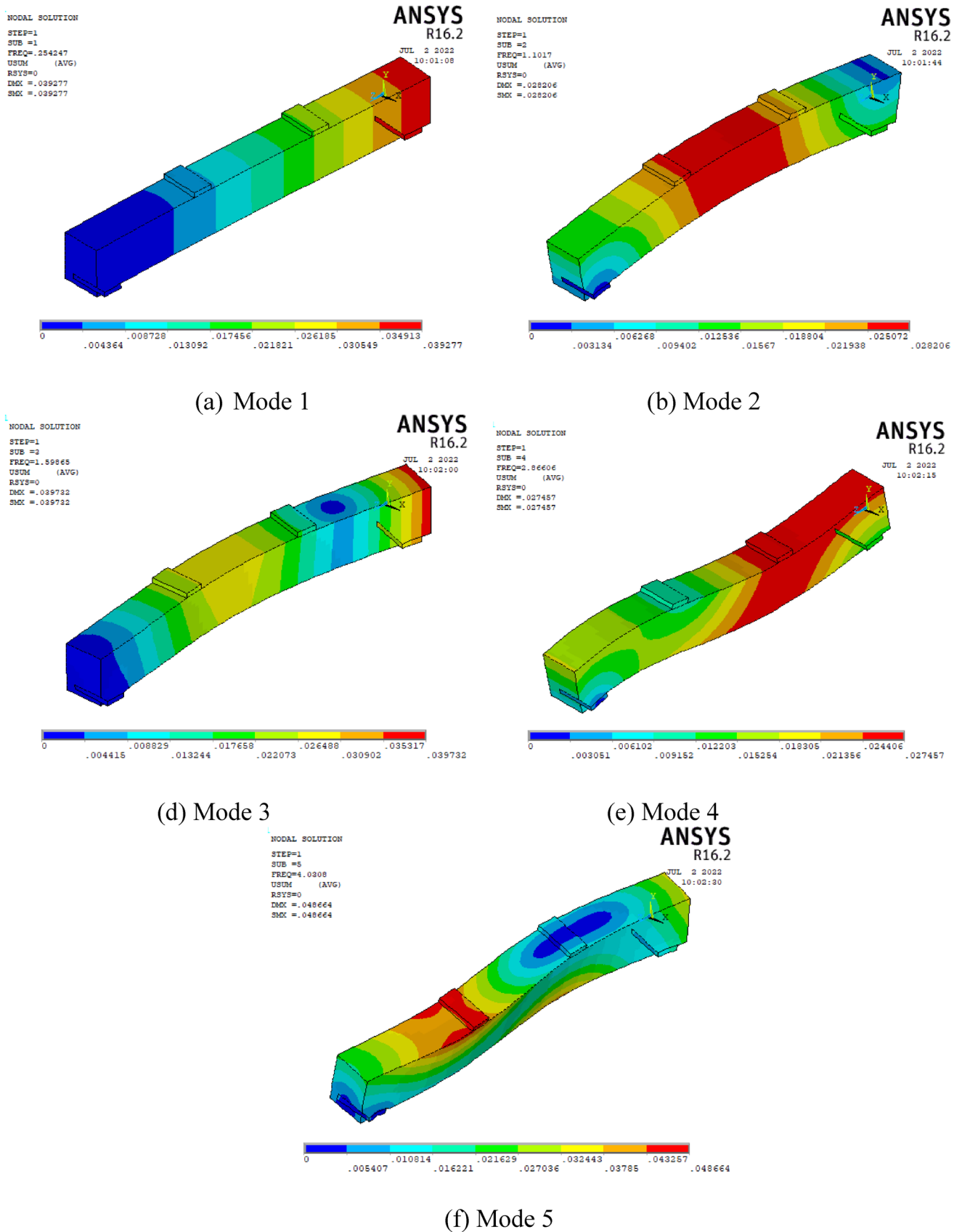


Fig. 17 Mode shapes under free vibration analysis

**Table 7** Natural frequency and displacement results

Modes	Tension controlled		Transition controlled		Compression controlled	
	Freq. (Hz)	Disp. (mm)	Freq. (Hz)	Disp. (mm)	Freq. (Hz)	Disp. (mm)
1	0.254	0.039	0.256	0.039	0.260	0.039
2	1.102	0.028	1.112	0.028	1.136	0.028
3	1.599	0.040	1.605	0.040	1.632	0.040
4	2.866	0.027	2.889	0.027	2.943	0.027
5	4.031	0.0487	4.043	0.049	4.070	0.049

1.08 and 1.09 for the ultimate moment and deflection. This indicates that the proposed numerical model predicted closer results to the experimental data.

**Supplementary Information** The online version contains supplementary material available at <https://doi.org/10.1007/s42107-023-00789-w>.

**Acknowledgements** Not applicable

**Author's contributions** The corresponding author, Dr. P ideas, development, and design of methodology, formal analysis software, and mathematical analysis and writing-original draft preparation. YDR: data curation, writing, editing, and formal analysis software and mathematical analysis. IGK: visualization and investigation, writing-reviewing, editing, and supervision. The authors read and approved the final manuscript.

**Funding** The authors declare that no funding has been received for this work.

**Data availability** The data generated or analyzed in this study are presented in this article.

## Declarations

**Conflict of interest** The authors confirm that they don't have any competing interests.

**Ethical approval and consent to participate** Ethics and consent to this journal are not applicable.

**Consent for publication** All the authors are aware and agree to submit the manuscript to this journal.

## References

- Ahmad, N. A., & Salleh, N. (2022). Finite element modelling of reinforced concrete beams with a hybrid combination of steel and glass polymer reinforcement. *Recent Trends in Civil Engineering and Built Environment*, 3(1), 1928–1939.
- Al-Rousan, R. Z., Alhassan, M., & Al-wadi, R. (2020). Nonlinear finite element analysis of full-scale concrete bridge deck slabs reinforced with FRP bars. *Structures*, 27, 1820–1831.
- Bui, L. V. H., Stitmannathum, B., & Ueda, T. (2018). Ductility of concrete beams reinforced with both fiber-reinforced polymer and steel tension bars. *Journal of Advanced Concrete Technology*, 16(11), 531–548.
- Buyukkaragoz, A. L. P. E. R., Kalkan, I., & Lee, J. H. (2013). A numerical study of the flexural behavior of concrete beams reinforced with AFRP bars. *Strength of Materials*, 45(6), 716–729.
- Choobbor, S. S., Hawileh, R. A., Abu-Obeidah, A., & Abdalla, J. A. (2019). Performance of hybrid carbon and basalt FRP sheets in strengthening concrete beams in flexure. *Composite Structures*, 227, 111337.
- Committee, A. C. I. (2019). *Building code requirements for structural concrete and commentary (ACI 318–19)*. USA: Farmington Hills, MI, American Concrete Institute.
- Godínez-Domínguez, E. A., Tena-Colunga, A., & Juárez-Luna, G. (2015). Nonlinear finite element modeling of reinforced concrete haunched beams designed to develop a shear failure. *Engineering Structures*, 105, 99–122.
- Hamrat, M., Bouziadi, F., Boulekbache, B., Daouadji, T. H., Chergui, S., Labeled, A., & Amziane, S. (2020). Experimental and numerical investigation on the deflection behavior of pre-cracked and repaired reinforced concrete beams with fiber-reinforced polymer. *Construction and Building Materials*, 249, 118745.
- Hawileh, R. A. (2015). Finite element modeling of reinforced concrete beams with a hybrid combination of steel and aramid reinforcement. *Materials & Design*, 1980–2015(65), 831–839.
- Hawileh, R. A., Abdalla, J. A., & Naser, M. Z. (2019). Modeling the shear strength of concrete beams reinforced with CFRP bars under unsymmetrical loading. *Mechanics of Advanced Materials and Structures*, 26(15), 1290–1297.
- Hussein, L. F., Khattab, M. M., & Farman, M. S. (2021). Experimental and finite element studies on the behavior of hybrid reinforced concrete beams. *Case Studies in Construction Materials*, 15, e00607.
- Kaveh, A. (2014). *Computational structural analysis and finite element methods*. Springer International Publishing.
- Kaveh, A., Dadras Eslamlou, A., Javadi, S. M., & Geran Malek, N. (2021). Machine learning regression approaches for predicting the ultimate buckling load of variable-stiffness composite cylinders. *Acta Mechanica*, 232, 921–931.
- Kaveh, A., & Khalegi, A. (1998). Prediction of strength for concrete specimens using artificial neural networks. *Advances in Engineering Computational Technology*, 45, 165–171.
- Kaveh, A., & Khavaninzadeh, N. (2023). June. Efficient training of two ANNs using four meta-heuristic algorithms for predicting the FRP strength. *Structures*, 52, 256–327.
- Kaya, N., & Anil, Ö. (2021). Prediction of load capacity of one way reinforced concrete slabs with openings using nonlinear finite element analysis. *Journal of Building Engineering*, 44, 102945.
- Mechanical, A. N. S. Y. S. (2016). A finite element computer software and user manual for nonlinear structural analysis. *Mechanical APDL Release*, 18, 223.
- Mustafa, S. A., & Hassan, H. A. (2018). Behavior of concrete beams reinforced with hybrid steel and FRP composites. *HBRC Journal*, 14(3), 300–308.
- Osman, B. H., Wu, E., Ji, B., & Abdulhameed, S. S. (2017). Shear behavior of reinforced concrete (RC) beams with circular web



- openings without additional shear reinforcement. *KSCE Journal of Civil Engineering*, 21(1), 296–306.
- Özcan, D. M., Bayraktar, A., Şahin, A., Haktanir, T., & Türker, T. (2009). Experimental and finite element analysis on the steel fiber-reinforced concrete (SFRC) beams ultimate behavior. *Construction and Building Materials*, 23(2), 1064–1077.
- Pandimani. (2023). Computational modeling and simulations for predicting the nonlinear responses of reinforced concrete beams. *Multidiscipline Modeling in Materials and Structures*, 19(4), 728–747.
- Pandimani, P. (2022). Finite-element modeling of partially prestressed concrete beams with unbonded tendon under monotonic loadings. *Journal of Engineering, Design and Technology*. <https://doi.org/10.1108/JEDT-09-2021-0495>
- Pandimani, P., & M.R. and Geddada, Y. (2022). Numerical nonlinear modeling and simulations of high strength reinforced concrete beams using ANSYS. *Journal of Building Pathology and Rehabilitation*, 7(1), 1–23.
- Pandimani, P., Ponnada, M. R., & Geddada, Y. (2021a). A comprehensive nonlinear finite element modelling and parametric analysis of reinforced concrete beams. *World Journal of Engineering*, 22, 44.
- Ponnada, M. R., & Geddada, Y. (2021b). Nonlinear modelling and finite element analysis on the load-bearing capacity of RC beams with considering the bond–slip effect. *Journal of Engineering, Design and Technology*. <https://doi.org/10.1108/JEDT-06-2021-0310>
- Rofooei, F. R., Kaveh, A., & Farahani, F. M. (2011). Estimating the vulnerability of the concrete moment resisting frame structures using artificial neural networks. *Int J Optim Civil Eng*, 1(3), 433–448.
- Sayed, A. M. (2019). Numerical study using FE simulation on rectangular RC beams with vertical circular web openings in the shear zones. *Engineering Structures*, 198, 109471.
- Indian Standard, IS 456, (2000). Plain and reinforced concrete code of practice. New Delhi: Bureau of Indian Standards.
- Vasudevan, G., & Kothandaraman, S. (2014). Experimental investigation on the performance of RC beams strengthened with external bars at soffit. *Materials and Structures*, 47(10), 1617–1631.
- Vasudevan, G., Kothandaraman, S., & Azhagarsamy, S. (2013). Study on non-linear flexural behavior of reinforced concrete beams using ANSYS by discrete reinforcement modeling. *Strength of Materials*, 45(2), 231–241.
- Willam, K. J. (1975). Constitutive model for the triaxial behaviour of concrete. *Proc. Intl. Assoc. Bridge Structl. Engrs*, 19, 1–30.
- Wolanski, A.J., (2004). Flexural behavior of reinforced and prestressed concrete beams using finite element analysis Doctoral dissertation, Marquette University.
- Xiaoming, Y., & Hongqiang, Z. (2012). Finite element investigation on load carrying capacity of corroded RC beam based on bond-slip. *Jordan Journal of Civil Engineering*, 6(1), 134–146.
- Yousaf, M., Siddiqi, Z. A., Sharif, M. B., & Qazi, A. U. (2017). Force- and displacement-controlled non-linear FE analyses of RC beam with partial steel bonded length. *International Journal of Civil Engineering*, 15(4), 499–513.

**Publisher's Note** Springer Nature remains neutral with regard to jurisdictional claims in published maps and institutional affiliations.

Springer Nature or its licensor (e.g. a society or other partner) holds exclusive rights to this article under a publishing agreement with the author(s) or other rightsholder(s); author self-archiving of the accepted manuscript version of this article is solely governed by the terms of such publishing agreement and applicable law.